

A Neural Network Method for Mixture Estimation for Vegetation Mapping

Gail A. Carpenter,^{*} Sucharita Gopal,[†] Scott Macomber,[†]
Siegfried Martens,^{*} and Curtis E. Woodcock[†]

While most forest maps identify only the dominant vegetation class in delineated stands, individual stands are often better characterized by a mix of vegetation types. Many land management applications, including wildlife habitat studies, can benefit from knowledge of mixes. This article examines various algorithms that use data from the Landsat Thematic Mapper (TM) satellite to estimate mixtures of vegetation types within forest stands. Included in the study are maximum likelihood classification and linear mixture models as well as a new methodology based on the ARTMAP neural network. Two paradigms are considered: classification methods, which describe stand-level vegetation mixtures as mosaics of pixels, each identified with its primary vegetation class; and mixture methods, which treat samples as blends of vegetation, even at the pixel level. Comparative analysis of these mixture estimation methods, tested on data from the Plumas National Forest, yields the following conclusions: 1) Accurate estimates of proportions of hardwood and conifer cover within stands can be obtained, particularly when brush is not present in the understory; 2) ARTMAP outperforms statistical methods and linear mixture models in both the classification and the mixture paradigms; 3) topographic correction fails to improve mapping accuracy; and 4) the new ARTMAP mixture system produces the most accurate overall results. The Plumas data set has been made available to other researchers for further development of new mapping methods and comparison with the quantitative studies presented here,

which establish initial benchmark standards. ©Elsevier Science Inc., 1999

INTRODUCTION: ESTIMATING VEGETATION MIXTURES

Fundamental to remote sensing methodology is the fact that sensor readings are integrated over a given area, or pixel. However, limits on the implied hypothesis of landscape uniformity within a pixel have long been observed. One way to define the issue uses the dichotomy proposed by Strahler et al. (1986) to characterize the relationship between the size of landscape units and the pixel. In this formulation, a *high(H)-resolution* condition features landscape units that are significantly larger than pixels, so that pixels may be accurately considered representative samples from larger populations. The alternative *low(L)-resolution* case features units that are smaller than pixels, so that each pixel typically represents a mixture of landscape components.

Corresponding to the high-/low-resolution dichotomy of the landscape is a mapping method dichotomy: *classification methods* assign a single label to each pixel, and *mixture methods* assign fractional labels to each pixel. This article compares these two classes of methods in a single setting. To accomplish this goal, a new database, designed for this purpose, was collected in the Plumas National Forest. Quantitative studies investigate site-level vegetation mixture estimation capabilities of both classification and mixture methods. Among the mixture methods is a new neural network paradigm, introduced here. Topographic correction was also tested, but this input preprocessing step failed to improve the mapping accuracy of any system. These analyses establish a set of benchmark performance measures. To facilitate comparison with other methods, the Plumas database has

^{*} Center for Adaptive Systems and Department of Cognitive and Neural Systems, Boston University, Boston

[†] Center for Remote Sensing and Department of Geography, Boston University, Boston

Address correspondence to Gail A. Carpenter, Dept. of Cognitive and Neural Systems, 677 Beacon St., Boston Univ., Boston, MA 02215. E-mail: gail@cns.bu.edu

Received 21 September 1998; revised 24 March 1999.

been made publicly available for ongoing research and development (plumas@crsa.bu.edu).

Classification Methods: Maximum Likelihood and ARTMAP

Image classification has been used for decades to produce vegetation maps. In many respects these maps resemble the thematic maps produced from interpretation of aerial photography, with each location characterized by a single vegetation type (Strahler, 1981). In addition, image classification has been used at times to estimate mixes of vegetation types, usually at the scale of vegetation stands that include many remotely sensed pixels. In one approach, each pixel in a stand is characterized by a single vegetation type. The stand-level fraction of a vegetation type is then predicted to be the proportion of pixels assigned to that class. Woodcock et al. (1996) assessed the accuracy of this approach for providing secondary vegetation types within individual stands using Landsat TM imagery. Stenback and Congalton (1990) used image classification to detect shrubs in the understory of conifer forests by labeling unsupervised clusters with respect to both canopy overstory characteristics and the presence of understory shrubs.

A variation on this theme uses the distributed output signal of a classification algorithm to characterize mixtures within pixels. A pixel label might then represent the strength of association with or probability of membership in classes, rather than a single category. Statistical classifiers such as maximum likelihood (Marsh et al., 1980; Foody et al., 1992) and neural networks (Foody, 1996; Moody et al., 1996) have been applied in this way. The approach is related to fuzzy set theory, since an individual pixel may be viewed as having degrees of membership in multiple classes (Robinson 1988; Fisher and Pathirana, 1990).

This article evaluates two types of classification methods for mixture estimation: the maximum likelihood algorithm and the ARTMAP neural network (Carpenter et al., 1991; 1992). Maximum likelihood is a standard algorithm (Richards, 1993) in the remote sensing literature. Introduced more recently, ARTMAP is already being used in a variety of application settings, including industrial design and manufacturing, robot sensory motor control and navigation, machine vision, and medical imaging (Carpenter, 1997), as well as remote sensing (Carpenter et al., 1997). ARTMAP belongs to the family of adaptive resonance theory (ART) networks, which are characterized by their ability to carry out fast, stable, on-line learning, recognition, and prediction. These features differentiate ARTMAP from the family of feed-forward multilayer perceptrons (MLPs), including backpropagation, which typically require slow, off-line learning. The inherent instability of MLP learning may make such a system unsuitable for large-scale, unconstrained mapping

problems. ARTMAP systems self-organize arbitrary mappings from input vectors, representing features such as spectral values and terrain variables, to output vectors, representing predictions such as vegetation classes or environmental variables. Internal ARTMAP control mechanisms create stable recognition categories of optimal size by maximizing code compression while minimizing predictive error.

Mixture Methods: Endmembers and ARTMAP

Mixture models postulate “blender” dynamics, which mix vegetation types at the pixel scale as well as at the stand scale. One such method is *spectral mixture analysis* (Adams et al., 1986). The *sma* program in IPW (Frew, 1990) was used here for the linear mixture analysis, with singular value decomposition (unconstrained).

The linear mixture model is defined in terms of a set of *image endmembers*, with mixture compositions calculated by linear interpolation within the convex set defined by the endmembers. In the Plumas application, endmembers represent the mean spectrum of TM bands averaged over all pixels in selected “pure” stands, which are dominated by single vegetation types. Note, however, that even the pure stands are mixtures in their own right. A conifer forest stand, for example, is at least a mixture of sunlit tree crown, shadowed tree crown, and background visible through gaps in the canopy. Two types of endmember sets were tested. The first set represents the most extreme, or *exterior*, spectral values for conifer, hardwood, and barren stands. The second set of *interior* endmembers solves some specific problems that arose when using the exterior endmembers (see Discussion).

The spectral mixture method has proved successful in many applications, particularly with hyperspectral imagery (with many spectral bands) and when the materials to be estimated are elemental (e.g., mineral constituents in rocks and soils) (Adams et al., 1993). This method has been used for vegetation analysis, but most such applications seek to quantify proportions of broadly defined components such as bare soil, photosynthetic vegetation, nonphotosynthetic vegetation, and shadow (Smith et al., 1990; Roberts et al., 1993; Ray and Murray, 1996), rather than the life-form components of a vegetation mix. Adams et al. (1995), measuring land-cover change in the Amazon, use endmember fractions to produce a thematic map, evidently the first use of linear mixture analysis for this purpose.

In summary, in the past, endmembers have typically represented fundamental classes, such as *vegetation*, *soil*, and *shade*, rather than vegetation types, such as *conifer* and *hardwood*. For the Plumas vegetation mapping problem, performance of the spectral mixture model is compared with that of an ARTMAP neural network, introduced here, that estimates fractions of classes within pixels. During learning, mixture ARTMAP associates a

site-level vegetation fraction with each training set pixel. Output resolution is determined by a free parameter, called *vigilance*, described in the system algorithm. A small vigilance value produces a coarse-resolution system, which might predict *low/medium/high* vegetation fractions; while a larger vigilance value produces a fine-resolution system, which would more closely track precise field measurements. During testing, fractional pixel-level vegetation class outputs are averaged across all pixels at a given site to obtain the site-level mixture prediction.

MATERIALS: THE PLUMAS NATIONAL FOREST DATA SET

Field Observations and Measurements

The setting of the present study, the Plumas National Forest, is located at the northern tip of the Sierra Nevada Mountains in California. The Plumas National Forest covers a large area (over 45,000 km²) which is topographically and climatically diverse. This region is characterized by temperate conifer forests mixed with chaparral brush fields and deciduous and evergreen hardwood forests. Dominant species of conifers include Jeffrey pine (*Pinus jeffreyi*), white fir (*Abies concolor*), red fir (*Abies magnifica*), Douglas fir (*Pseudotsuga menziesii*), ponderosa pine (*Pinus ponderosa*), and sugar pine (*Pinus lambertiana*). The dominant hardwood species are the winter-deciduous black oak (*Quercus kelloggii*) and the evergreen canyon live oak (*Quercus chrysolepis*). Willows (*Salix* spp.) and alders (*Alnus* spp.) also occur, frequently in dense thickets. For purposes of vegetation mapping for forest management, the primary goal is quantification of mixes of needle-leafed conifers and broadleafed hardwoods within stands. Quantification of the fraction of brush understory in forest stands would also be useful.

For the Plumas study, field data were collected in August 1995 at 388 widely distributed stands. The stands were delineated on 1:15,840 scale color aerial photographs and visited in the field. Sites range in size from 11 pixels to 224 pixels, with an average of 52 pixels per site. The primary data set used for mixture analysis includes estimates of conifer and hardwood crown cover within each stand, which were derived from close visual inspection of aerial photographs while traversing the stands (Woodcock et al., 1994). This data collection method allows large numbers of stands to be surveyed in a relatively short time period, but also implies that the field measurements contain a margin of error. Each ground truth vegetation fraction in the data set represents a consensus. By comparing typical measurements first reported independently by members of the field crew, the error bound was estimated to be 10%. Results of the analyses below should be viewed in light of this expected measurement error.

Image Data

The satellite sensor data in this study are from a 20 June 1990 Landsat TM image. The image was registered to a map projection and resampled using a nearest neighbor algorithm. Mapping studies use as system input the six spectral bands TM1–5 and TM7. Classification and mixture methods were tested on both the original spectral data and on data that had been corrected for topographic effects, as follows.

Topographic Correction

One factor complicating the task of extracting information from multispectral imagery is the *topographic effect*. That is, surface reflectance in mountainous terrain varies as a function of surface properties, slope, and aspect, due primarily to changes in amounts of incident solar radiation and the anisotropic reflectance of vegetated surfaces. The magnitude of the topographic effect depends upon solar elevation, surface slope aspect, and inclination (Holben and Justice, 1980; Justice et al., 1981). If the effects of topography could be removed from the data, the brightness values in the image would be changed into what they would have been if the surface were flat.

Several methods for correcting terrain effects have been used in remote sensing applications (Smith et al., 1980; Holben and Justice, 1980; Justice et al., 1981; Lee and Kaufman, 1986; Civco, 1989; Proy et al., 1989; Naugle and Lashlee, 1992; Gu and Gillespie, 1998). One simple topographic correction method divides each observed brightness value by the cosine of the illumination angle (i), as if the surface were a lambertian reflector (Smith et al., 1980). That is,

$$L_{\text{norm}i} = \frac{L_{\text{obs}i}}{\cos i},$$

where $L_{\text{norm}i}$ equals the normalized brightness value, $L_{\text{obs}i}$ equals the observed brightness value, and the incidence angle i equals the angle between the Sun and the normal to the surface. This topographic correction method does not generally improve classifications, since many areas are either overcorrected or undercorrected (Naugle et al., 1992).

An alternative approach, applied here, takes into account nonlambertian reflectance properties, using an empirically derived *Minnaert coefficient* k (Smith et al., 1980). That is,

$$L_{\text{norm}i} = \frac{L_{\text{obs}i} \cos e}{(\cos i \cos e)^k},$$

where the *exitance angle* e equals the angle between the satellite (viewer) and the normal to the surface. The coefficient k would equal 1 for a lambertian surface and decrease toward 0 as surface anisotropy increases. Taking the log of both sides of this equation produces a linear form which can be used to estimate k in a linear regression model. That is,

Table 1. Minnaert Coefficients, for Topographic Correction

	Band 1	Band 2	Band 3	Band 4	Band 5	Band 7
k	0.207	0.288	0.227	0.763	0.604	0.445
R^2	0.280	0.264	0.068	0.337	0.205	0.060

$$y=b+kx,$$

where $y=\log(L_{\text{obsz}} \cos e)$, $b=\log(L_{\text{normz}})$, and $x=\log(\cos i \cos e)$. The coefficient k equals the slope of the regression line.

Values for k vary as a function of wavelength and surface properties, so that this method is most effective when different k values are applied for different land cover types (Justice et al., 1981; Smith et al., 1980). However, the present application seeks to develop and test efficient, automated mapping methods which do not rely on *a priori* knowledge of land cover types and thus one k value for each spectral band is used for corrections across the entire image. Values of k derived for all surface types resulted in low R^2 regression values, ranging between 0.04 and 0.10. These low R^2 values indicate that the k values would be ineffective for removing the topographic effect (Justice et al., 1981). To address this problem, only pixels from conifer sites were used to calculate the k values, which results in higher R^2 values. These constants k (Table 1) were derived for each of the six TM Bands 1–5 and 7, using the topographic slope and aspect calculated from registered digital terrain data.

All methods used to estimate mixtures within vegetation stands (maximum likelihood classification, ARTMAP classification, linear mixture analysis, and the ARTMAP mixture system) were tested using both the original spec-

tral values from the Landsat TM image data and the topographically corrected versions of the input data.

PERFORMANCE EVALUATION

Data Set Organization: With and Without Brush

Recall that image endmembers for the linear mixture analysis were selected from the set of “pure” stands. Figure 1 shows, for each pure stand, values of TM Band 3 (red) and TM Band 4 (near-infrared), and values of Band 4 and Band 5 (mid-IR). These band combinations were selected for the graphs as best illustrating the spectral separability of the vegetation types. Figure 1 shows that the patterns in reflectance of the hardwood, conifer, and barren classes show promise for spectral mixture analysis since they form a “well-conditioned simplex” (Nalepka and Hyde, 1972). This means that no vegetation type lies between any other two vegetation types. However, this separation does not hold for brush stands, which exhibit reflectance patterns that could have arisen from mixes of the other three vegetation types. Thus, finding the brush component of stands promises to be a difficult problem.

As a result of these observations, mixture analysis was carried out in two phases. The first phase considers only a smaller data set, which includes the 263 sites with hardwood, conifer, and barren ground alone, with no brush present. The second phase considers a larger data

Figure 1. Cosppectral plots for TM Bands 3, 4 and TM Bands 4, 5 of 40 pure sites show conifer (C), hardwood (H), and barren (B) to be fairly well clustered. However, the 10 brush sites (•) are mixed in among the others. The plots also show exterior and interior endmembers, which are connected by lines. Pure sites labeled barren and brush are defined as having no tree cover; conifer sites have no hardwood cover; hardwood sites have less than 10% conifer cover; and hardwood and conifer sites have no brush.

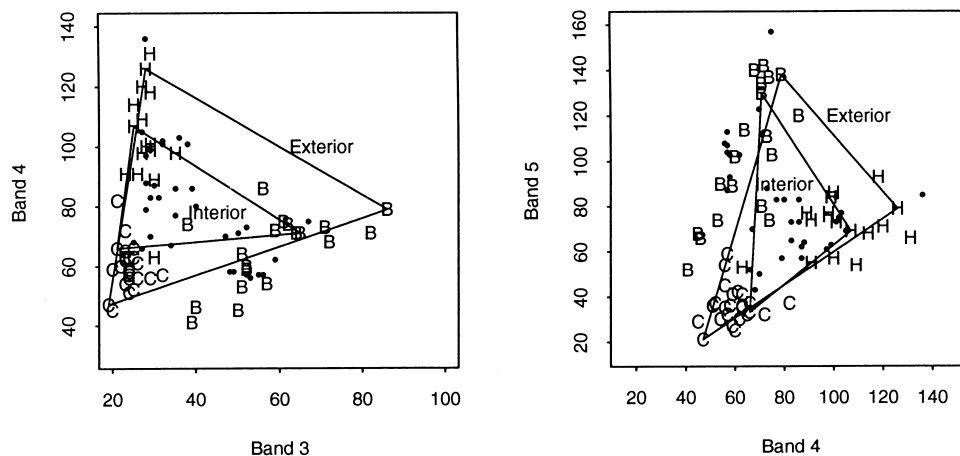


Table 2. Predictive Accuracy of Classification (ML and ARTMAP) and Mixture (Exterior, Interior, and ARTMAP) Systems for the Small Data Set^a

	a) Original Input Data					b) With Topographic Correction				
	RMS Error			% Total Predictions within 10%	% Total Predictions within 20%	RMS Error			% Total Predictions within 10%	% Total Predictions within 20%
	C	H	Barren			C	H	Barren		
ML classification	0.25	0.14	0.24	41%	74%	0.25	0.15	0.23	37%	76%
ARTMAP classification	0.17	0.11	0.15	55%	89%	0.17	0.12	0.14	59%	89%
Exterior mixture	0.20	0.15	0.24	27%	76%	0.27	0.15	0.23	32%	73%
Interior mixture	0.21	0.09	0.21	46%	83%	0.23	0.21	0.19	27%	76%
ARTMAP mixture	0.15	0.10	0.12	65%	96%	0.15	0.10	0.12	66%	95%

^a Optimal estimates are indicated in boldface type.

set, which includes the first set of 263 stands plus 125 stands with brush. In the field data, sites were identified as *with brush* or *without brush*, but a separate estimate of the brush fraction was not made. Instead, the fraction of *barren+brush* was estimated as a unit. In tests, therefore, systems predict a *conifer/hardwood/other* mixture, where *other* represents *barren* in the small data set and *barren+brush* in the large data set. Including the brush sites makes the mapping task more difficult and more realistic.

Performance Measures

Comparative performance of all systems was evaluated in terms of the root mean squared (RMS) error. For a given life-form class (*conifer/hardwood/other*), the RMS error with respect to that class is

$$\text{RMS error} \equiv \sqrt{\frac{\sum_{i=1}^n (y_i - x_i)^2}{n}},$$

where n is the number of test sites, y_i is the predicted cover proportion of the life-form for site i , and x_i is the actual cover proportion of the life-form, based on field measurements. A correlation coefficient error measure gave nearly identical patterns of results.

Training and testing protocols varied with the types of methods used. The maximum likelihood system was trained on a randomly selected sample of 10 pure sites for each vegetation class and tested on the remaining sites. For linear mixture methods, endmembers were chosen representing one pure site for each vegetation type (*conifer*, *hardwood*, *barren*), after inspection of all the pure sites. Mixture predictions were then enumerated for all sites.

ARTMAP training and testing was carried out using a fivefold cross-validation procedure (Mosier, 1951). This

standard statistical procedure ensures a strict separation between training and testing sets, and all reported results cite system performance on data not seen during training. Following the cross-validation protocol, the data set is partitioned into five disjoint subsets, each containing approximately 20% of all the sites. Each run uses one subset as the test set and the remaining four as the training set. Since ARTMAP employs fast learning, results can vary somewhat with the ordering of the training input. To average away this variation, the evaluation procedure was repeated 25 times for each training/testing subset partition, using a different randomly chosen input ordering each time.

The fact that cross-validation uses each of the five subsets, in turn, as a test set compensates for possible variations in the training/testing set partition. Thus reported ARTMAP mixture results reflect values averaged across 125 separate system training runs. With no selection made of an optimal test set, this procedure produces robust performance measures while ensuring that no test site is ever used in training.

RESULTS: MIXTURE ESTIMATION FOR THE SMALL DATA SET

Classification Method Performance

Table 2 summarizes results of vegetation mixture estimates on the small data set, which excludes sites with brush. Each system attempts to predict conifer (C), hardwood (H), and barren fractions in test set sites. For the classification methods, a system predicts a single vegetation class for each pixel. Table 2a shows that, using uncorrected input data, the root mean squared (RMS) errors for maximum likelihood (ML) are substantially higher than those for the ARTMAP classification system. Similarly, the numbers of predictions that fall within 10% and 20% of the field measurements are lower for

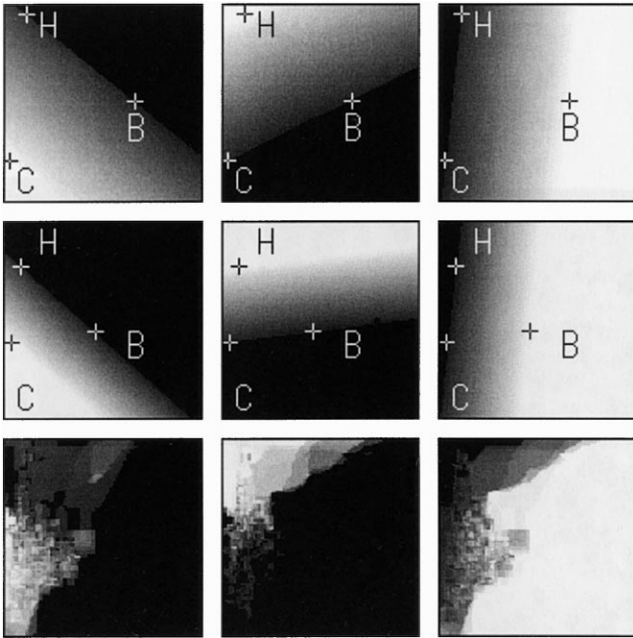


Figure 2. Mixture predictions of two linear mixture models (exterior and interior endmembers) and a neural network (ARTMAP mixture), plotted for TM Bands 3 (x -axis) and 4 (y -axis) without topographic correction. Columns show white areas estimating 100% *conifer* (C), *hardwood* (H), and *barren* (B). As the gray scale moves from white to black, the estimated percent of the designated life-form decreases from 100% to 0%. ARTMAP is seen to capture more complex features of the data than do the linear mixture models. Scale: 17–121 digital numbers (DN) (x -axis); and 26–130 DN (y -axis).

maximum likelihood than for ARTMAP. Table 2b shows that topographic correction does not significantly affect performance of the two classification methods.

Mixture Method Performance

Performance of the exterior endmember mixture model on the small data set is similar to that of the maximum likelihood classification methods, both without topographic correction (Table 2a) and with topographic correction (Table 2b). The RMS error rate of the exterior endmember mixture model is slightly better than that of the maximum likelihood system, but the number of predictions that fall within 10% of the field measurements is low. With topographic correction, interior endmember performance is also similar to these two. Without topographic correction, performance of the interior endmember mixture model is better, improving upon maximum likelihood classification performance in every measure. However, it is still worse than ARTMAP classification in all respects, except for a small improvement in the RMS error for hardwood. Performance of the ARTMAP mixture model is superior to that of all the others, as indicated by the boldface entries, which highlight the best item in each column. Two-thirds of the ARTMAP pre-

dictions fall within 10% of the field measurements, and almost all predictions fall within 20%. Since the bound on the data set measurement error is approximately 10%, Table 2 shows that a majority of the ARTMAP mixture estimates on the small data set are close to optimal.

Figure 2 illustrates qualitative differences in the life-form estimates of linear mixture models and an ARTMAP mixture system. The results displayed in this figure are for a simplified data set based on only two spectral bands (TM 3 and TM 4), to facilitate graphical representation. The columns show estimated fractions of *conifer*, *hardwood*, and *barren*, respectively, where bright values represent high fractions and dark values represent low fractions. The top two rows of Figure 2 show the exterior and interior endmember predictions from the linear mixture model, with endmember locations marked (+). The bottom row illustrates ARTMAP mixture prediction, which has a much higher degree of complexity than the other two approaches. Spectral mixture models allow only a straightforward linear decrease in the estimates of one endmember along a line perpendicular to the line connecting the other two. In contrast, the neural network patterns may be as intricate as the training set requires.

Figure 3 shows the distribution of *conifer*, *hardwood*, and *barren* mixture percents predicted by the three mixture methods at sites in the small data set. The x -axis marks the actual percent of the vegetation type, from field measurements; and the y -axis marks the estimated percent of each vegetation type. Perfect predictions lie on the diagonal. Lines in each graph also show which points lie within 20% of the correct values. A large fraction of the exterior endmember estimates are seen to lie far from the diagonal: the system often predicts a high life-form fraction where the actual number is low, and vice versa. The interior endmember mixture model results show an improved pattern, with predicted fractions tending to correlate better with the actual fractions. However, this model still consistently overestimates conifer and underestimates barren. In contrast, nearly all the ARTMAP mixture predictions fall within 20% of the actual value.

Figure 4a summarizes these same results in a different format. For each of the three mixture methods, the graph indicates how many predictions fall within a given percent of the field measurements. The vertical line at the 10% error bound depicts the 27%, 46%, and 65% of total predictions that fall within this criterion level for exterior, interior, and ARTMAP mixture methods, respectively, as shown in Table 2a. Similarly, the vertical line at the 20% error bound depicts the 76%, 83%, and 96% levels for the three methods. Figure 4a confirms that ARTMAP gives the most accurate mixture estimates, and further shows that maximal accuracy holds at every error criterion level. Exterior endmember prediction is least accurate at every error level. Figure 4b confirms

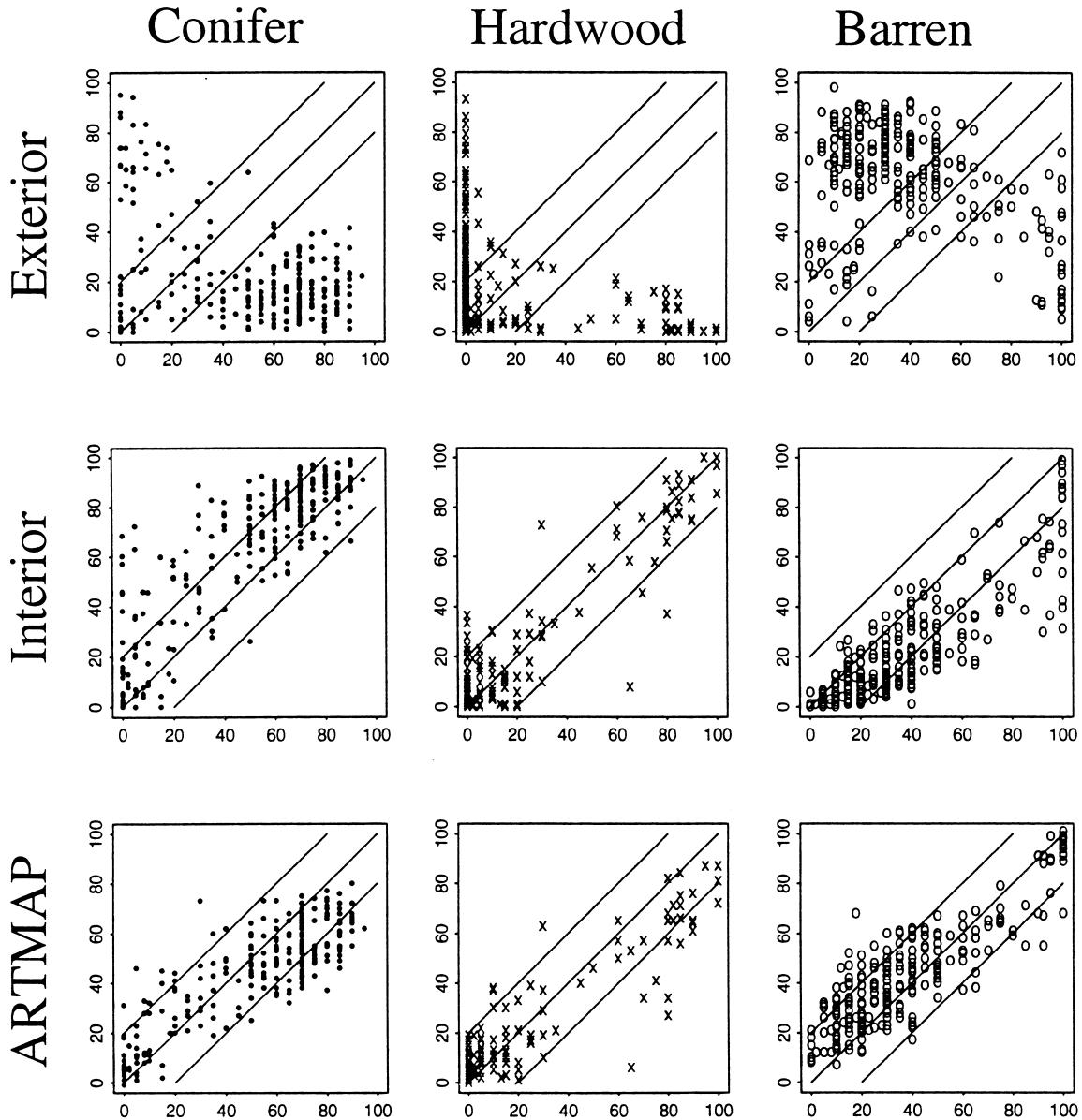


Figure 3. For the same nine combinations as in Figure 2, each plot compares the actual percent, based on field measurements (x-axis) with the predicted percent (y-axis) of a given life-form. Diagonal lines represent exactly correct estimates, and flanking lines enclose points that are within $\pm 20\%$ correct. Each point on a plot represents a site in the small data set, which excludes sites with brush, without topographic correction.

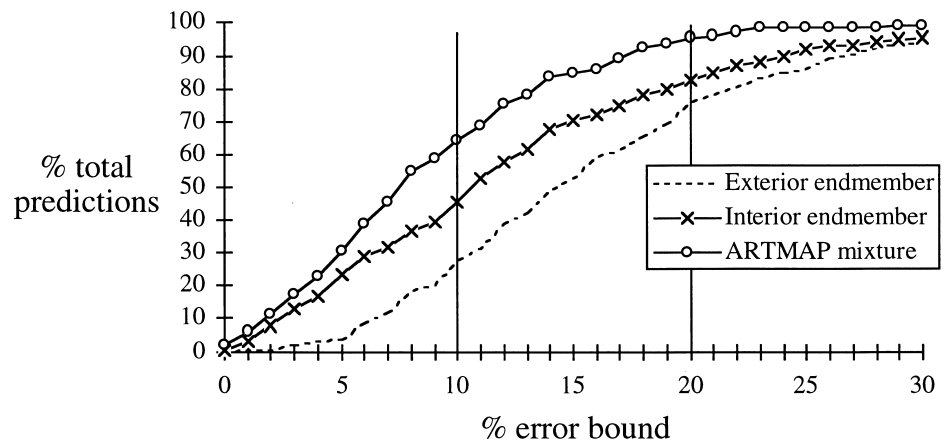
the observation that topographic correction causes interior endmember performance to drop to the level of exterior endmember performance, while ARTMAP predictions remain at their prior accuracy levels.

RESULTS: MIXTURE ESTIMATION FOR THE LARGE DATA SET

The large data set adds 125 sites that contain brush to the 263 sites of the small data set. A comparison between Table 2 and Table 3 shows that performance of

each method deteriorates on the large data set, as expected from the spectral properties of the pure brush sites (Fig. 1). In addition, for this more challenging and realistic task, performance of the linear mixture models drops more steeply than that of the other methods. While the interior endmember model without topographic correction still performs better than the exterior model (Table 3a), the number of estimates that fall within 10% and 20% of the field measurements is now less than the number for either classification method. As on the small data set, topographic correction does not

(a) Small input set: original data



(b) Small input set: with topographic correction

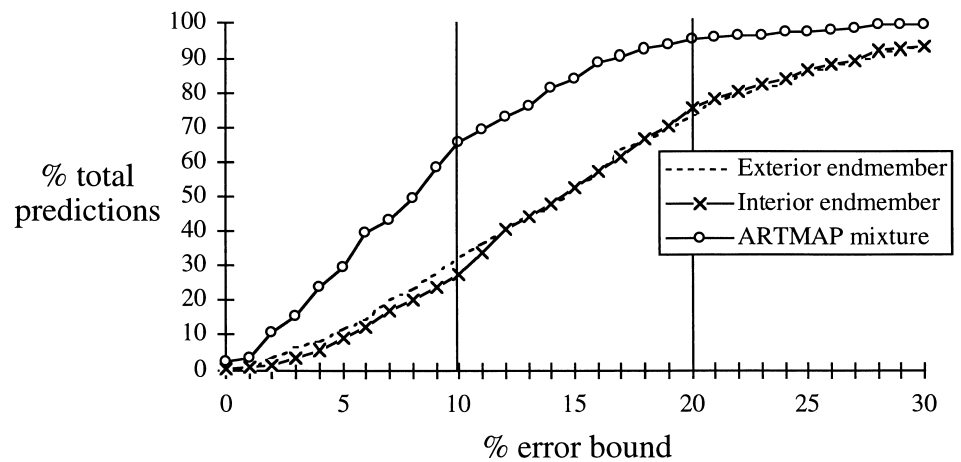


Figure 4. For three mixture prediction methods and for the small (no brush) data set, graphs show the percent of vegetation regions (conifer/hardwood/other) that lie within a given percent of the actual vegetation distribution: a) original input data; b) with topographic correction.

improve performance of any system (Table 3b). By every measure, predictive accuracy is best for the ARTMAP mixture method.

Comparing Figure 5 (large data set) with Figure 4 (small data set) indicates the widening gap between ARTMAP and the endmember mixture methods, as quantified in Table 2 and Table 3. Despite the difficulty of the problem of estimating mixture fractions with brush, 78% of the ARTMAP classification predictions fall within 20% of the field measurements and 84%(a)/83%(b) of the ARTMAP mixture predictions meet this criterion. For the other three methods, only 56–68% of the sites reach this level of accuracy.

DISCUSSION: SATELLITE REMOTE SENSING AND MIXTURE ESTIMATION

The use of two different sets of endmembers in the linear mixture analysis was based on the following line of

reasoning. The first set of endmembers tested were the “exterior” endmembers, which were the means in spectral measurement space of the pure stands at the extremes of the distributions for the three vegetation types (Fig. 1). However, the results indicate several effects that undermine the notion that all other stands are accurately characterized as convex combinations of these three. First, the hardwood column of Figure 3 shows that, for the small data set, the exterior linear mixture model incorrectly predicts a significant hardwood fraction for many conifer or barren sites, which have little or no hardwood cover. The first column of Figure 3 shows that, to a lesser extent, the models also predict significant conifer fractions for pure sites that have little or no conifer cover. Figure 2 helps explain this effect. As spectral values move along the line connecting the conifer and hardwood exterior endmembers, for example, the model estimates a linear change in the proportions of hardwood and conifer. However, because of the considerable spec-

Table 3. Predictive Accuracy of Classification (ML and ARTMAP) and Mixture (Exterior, Interior, and ARTMAP) Systems for the Large Data Set^a

	<i>a) Original Input Data</i>					<i>b) With Topographic Correction</i>				
	<i>RMS Error</i>			<i>% Total Predictions within 10%</i>	<i>% Total Predictions within 20%</i>	<i>RMS Error</i>			<i>% Total Predictions within 10%</i>	<i>% Total Predictions within 20%</i>
	<i>C</i>	<i>H</i>	<i>Barren+Brush</i>			<i>C</i>	<i>H</i>	<i>Barren+Brush</i>		
ML classification	0.28	0.21	0.33	38%	67%	0.26	0.22	0.33	37%	68%
ARTMAP classification	0.19	0.16	0.23	41%	78%	0.19	0.16	0.23	39%	78%
Exterior mixture	0.27	0.20	0.37	20%	56%	0.27	0.21	0.36	24%	56%
Interior mixture	0.28	0.17	0.34	34%	63%	0.23	0.29	0.32	21%	60%
ARTMAP mixture	0.18	0.13	0.20	50%	84%	0.17	0.13	0.20	54%	83%

^a Optimal estimates are indicated in boldface type.

tral variability among pure stands, many pure conifer sites lie along this line joining conifer and hardwood endmembers. The farther these stands are from the conifer endmember, the larger the hardwood fraction will be. Spectral variability among pure sites, as well as other factors such as illumination, therefore undermine the principle of an exterior endmember as a spectral representative on a single vegetation class.

The selection of interior endmembers was an attempt to solve this problem. At least without topographic correction, the interior endmembers improve performance, yielding lower RMS errors and higher fractions of sites that fall within 10% and 20% of field estimates compared to the exterior endmembers (Tables 2a and 3a). The model now more accurately predicts large conifer and hardwood fractions for sites that do, in fact, have large fractions, as seen by the many points lying near the diagonal on the right side of the interior conifer and interior hardwood graphs of Figure 3a.

However, the interior endmember method produces new problems. For example, conifer fractions for mixed stands are now frequently estimated to have conifer covers that exceed field estimates, as seen by the overwhelming majority of points that lie above the diagonal in the interior conifer graph of Figure 3. Figure 6 further illustrates this problem. In Figure 6, histograms show the distribution of conifer percents estimated by exterior and interior linear mixture models, by the ARTMAP mixture model, and by the field estimates. These graphs illustrate how exterior endmembers tend to underestimate fractions while interior endmembers tend to overestimate conifer fractions. On the other hand, the ARTMAP mixture model produces a distribution that more closely resembles that of the field data, one reason why ARTMAP produces the best results.

A key question remains concerning the causes of variability in pure stands. One possible effect concerns

shadowing. In all spectral bands, conifers appear dark, and hence any effect that makes a stand appear dark may increase the estimate of conifer cover. A first-order effect in this regard is topography. Given that the Plumas National Forest features high topographic relief, stands receiving differing amounts of solar illumination at the time of the satellite overpass would be expected to have different brightnesses in the resulting image. More shadowed slopes would appear darker than slopes that are oriented toward the sun at the time of the satellite overpass. As a result, one would expect a higher estimate for conifer for more shadowed stands, and vice versa, but this effect is not observed. Figure 7 shows a plot of errors in conifer estimates as a function of the local solar zenith angle. If shadowing were having a strong effect, one would expect large positive errors for low values of the cosine of the solar zenith angle and negative errors for values approaching 1. However, Figure 7 shows an even distribution of errors with respect to illumination effects. The fact that errors are uncorrelated with topography helps explain why topographic correction does not improve results.

The problem of correction of topographic effects in images remains among the most difficult in optical remote sensing. The crux of the problem is that the magnitude of correction required is a function of surface properties. In forested environments this includes both the general vegetation type and the structure of the forest canopy (Verstraete et al., 1990; Li and Strahler, 1992; Strahler, 1997). Thus, to correct for the topographic effects in images, it is necessary first to have both an accurate representation of the topography and information regarding vegetation type and structure. When trying to use remote sensing to recover this kind of information, a "chicken and egg" situation results.

Nonlinear effects have been mentioned frequently in the literature as possible sources of error in the results

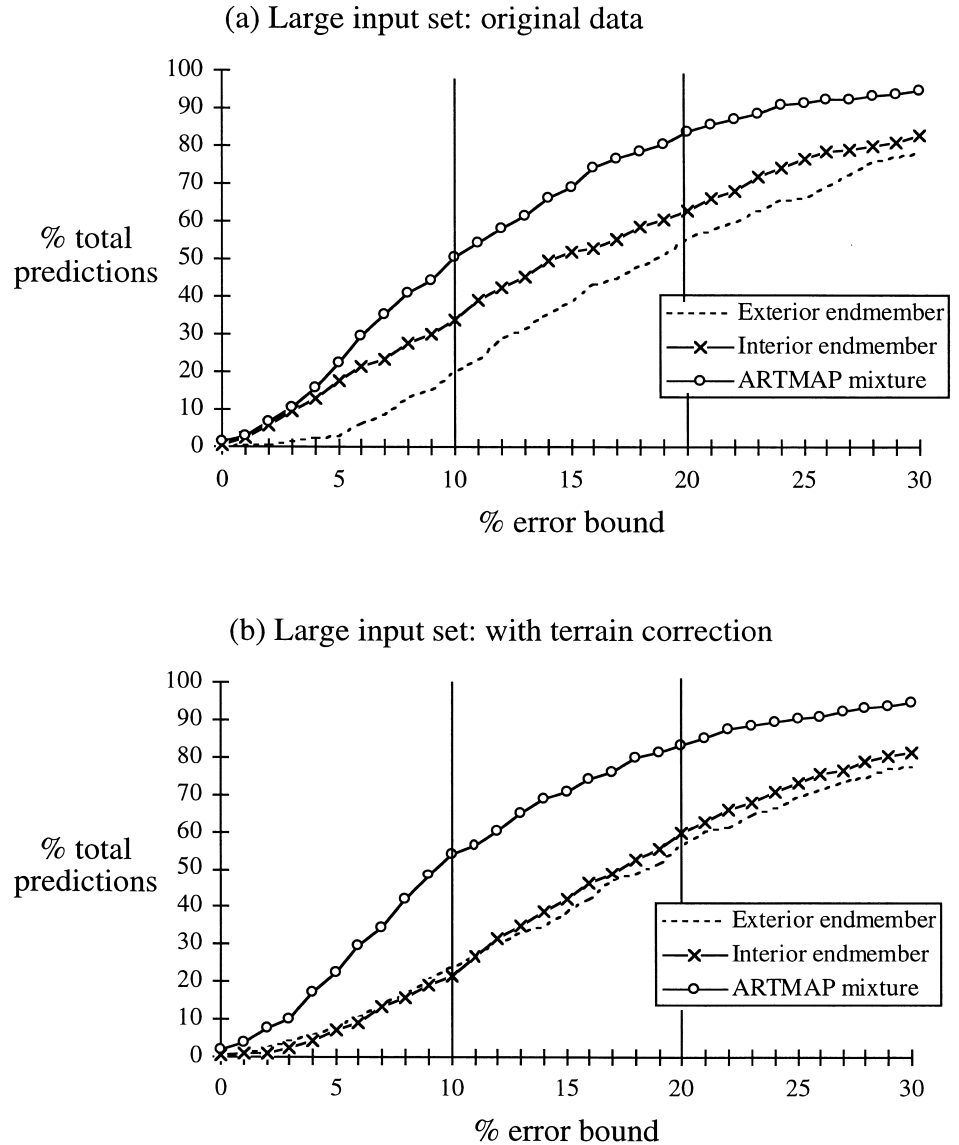


Figure 5. For three mixture prediction methods and for the large data set (with brush), graphs show the percent of vegetation regions (conifer/hardwood/other) that lie within a given percent of the actual vegetation distribution: a) original input data; b) with topographic correction.

of linear mixture models. The fact that ARTMAP has no inherent limitations in this respect helps explain why this system consistently produces the best results.

ARTMAP NEURAL NETWORK ALGORITHM FOR MIXTURE ESTIMATION

The following algorithm specifies a self-contained ARTMAP implementation for both the classification and the mixture estimation paradigms, first for training then for testing. Figure 8 depicts components of a real-time network architecture that would implement the algorithm. Table 4 lists variables from the network modules ART_a and ART_b. Table 5 lists system parameters, along with their domains and the values used in computer tests. A more expository explanation of the classification version of the algorithm, for remote sensing applications, can be found in Carpenter et al. (1997).

Training Set Input/Output Pairs

At ART_a, vector $\mathbf{a}=(a_1, a_2, a_3, a_4, a_5, a_6)$ represents the six spectral band values TM 1–5 and TM7 measured at a sample pixel, so that $M_a=6$. Component a_i represents the i th spectral band value, scaled to $[0,1]$. Each input to ART_a is *complement coded*. That is, the system input equals the concatenated vector $\mathbf{A}=(\mathbf{a}, \mathbf{a}^c)$, where $a_i^c \equiv 1-a_i$. Complement coding is a type of vector normalization, since

$$|\mathbf{A}| \equiv \sum_{i=1}^{2M_a} A_i = \sum_{i=1}^{M_a} a_i + \sum_{i=1}^{M_a} (1-a_i) = M_a.$$

At ART_b, vector $\mathbf{b}=(b_1, b_2, b_3)=(con, hwd, other)$ represents the vegetation class or the class mixture of the site, or stand, in which the sample pixel is located, so that $M_b=3$. For the small data set, *other=barren*; for the large data set, *other=barren+brush*. During ARTMAP classification training, one component of \mathbf{b} is 1, repre-

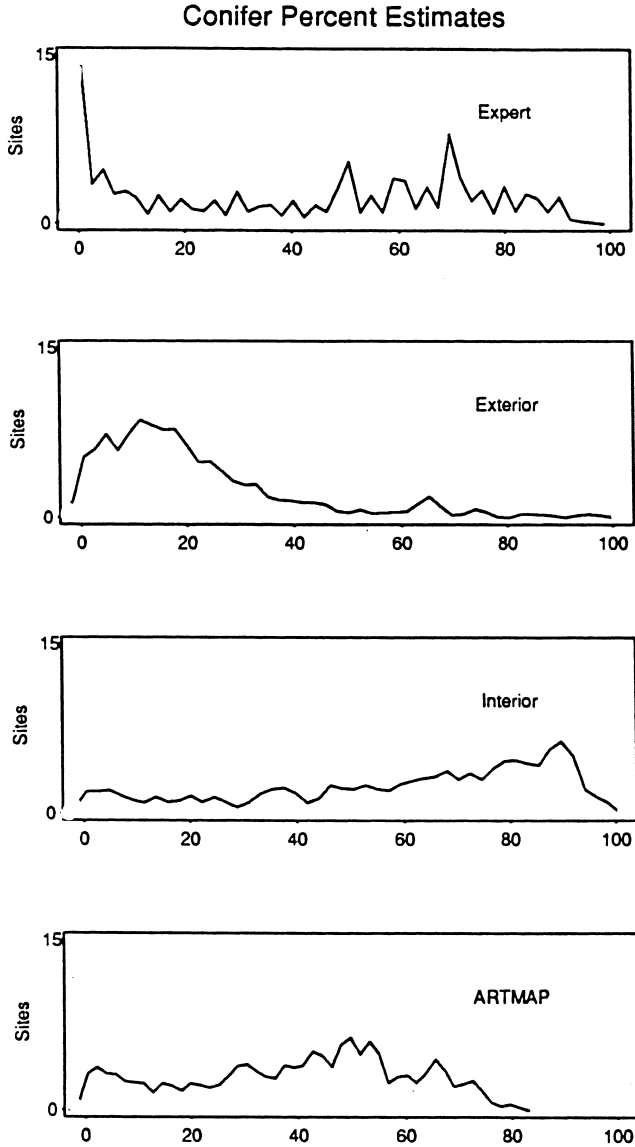


Figure 6. Distribution of conifer percent estimates by experts (field data) and by three mixture prediction models: exterior endmember, interior endmember, and ARTMAP mixture, on the small data set, without topographic correction. Note that the exterior endmember model predicts too many low-percent sites while the interior endmember model predicts too many high-percent sites. The ARTMAP distribution pattern is closest to that of the field data.

senting the most common vegetation class in the stand; and the other components are 0. For example, $\mathbf{b}=(1,0,0)$ for a stand with 70% conifer, 30% hardwood, and no barren ground or brush. During ARTMAP mixture training, the component b_l represents the fraction of the l th vegetation class in the stand, with $\sum_{l=1}^3 b_l=1$. For example, $\mathbf{b}=(0.7,0.3,0,0)$ represents a stand with 70% conifer and 30% hardwood.

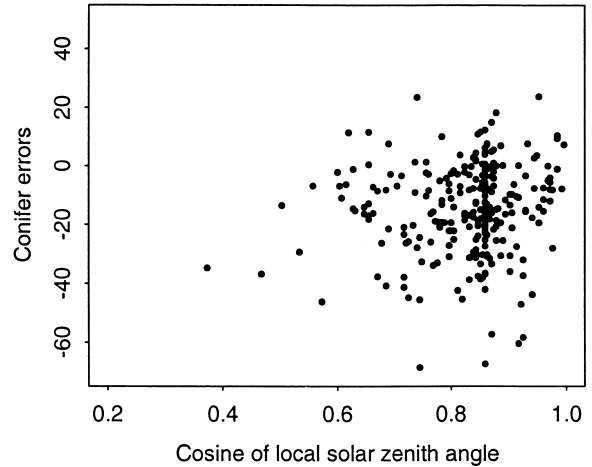


Figure 7. Conifer errors (mixture model–expert estimates) as a function of the cosine of local solar zenith angle. A strong effect from shadowing would cause large positive errors for small values of the local solar zenith angle and negative errors for values with the cosine close to 1. The graph shows a more random distribution of errors with respect to shadowing.

ARTMAP Training

During ARTMAP training, input/output pairs $(\mathbf{a}^{(1)}, \mathbf{b}^{(1)})$, $(\mathbf{a}^{(2)}, \mathbf{b}^{(2)})$, \dots , $(\mathbf{a}^{(n)}, \mathbf{b}^{(n)})$, \dots are presented for equal time intervals. Initially, all LTM variables are set equal to 1. That is, $w_{ij}^a=1$ for all i, j and $w_{lk}^b=1$ for all k, l .

Step 1—First input/output pair: Set $n=1$.

$$\text{Input vector}-A_i = \begin{cases} a_i^{(1)} & \text{if } 1 \leq i \leq M_a \\ 1-a_i^{(1)} & \text{if } M_a+1 \leq i \leq 2M_a \end{cases}$$

$$\text{Output vector}-b_l = b_l^{(1)} \quad (l=1 \dots M_b)$$

Set $C_a=1$, $C_b=1$, $J=1$, $K=1$, and $\kappa(1)=1$.

Go to **Step 7**.

Step 2—Compute the $F_1^b \rightarrow F_2^b$ signal: For $k=1 \dots C_b$, with $a \wedge b \equiv \min\{a, b\}$:

$$T_k^b = \frac{\sum_{l=1}^{M_b} b_l \wedge w_{lk}^b}{a + \sum_{l=1}^{M_b} w_{lk}^b}$$

Step 3—Choose an ART_b category K [(i) or (ii)]:

(i) *Committed node:* If $T_k^b \geq T^{b,u}$ for some F_2^b node $k=1 \dots C_b$, let K be the smallest index such that $T_k^b = \max\{T_1^b \dots T_{C_b}^b\}$.

$$F_1^b \text{ activation: } x_l^b = b_l \wedge w_{lk}^b \quad (l=1 \dots M_b)$$

If $\sum_{l=1}^{M_b} x_l^b < \rho_b$, set $T_k^b=0$ and go to **Step 3**.

Else go to **Step 4**.

(ii) *Uncommitted node:* If $T_k^b < T^{b,u}$ for all F_2^b

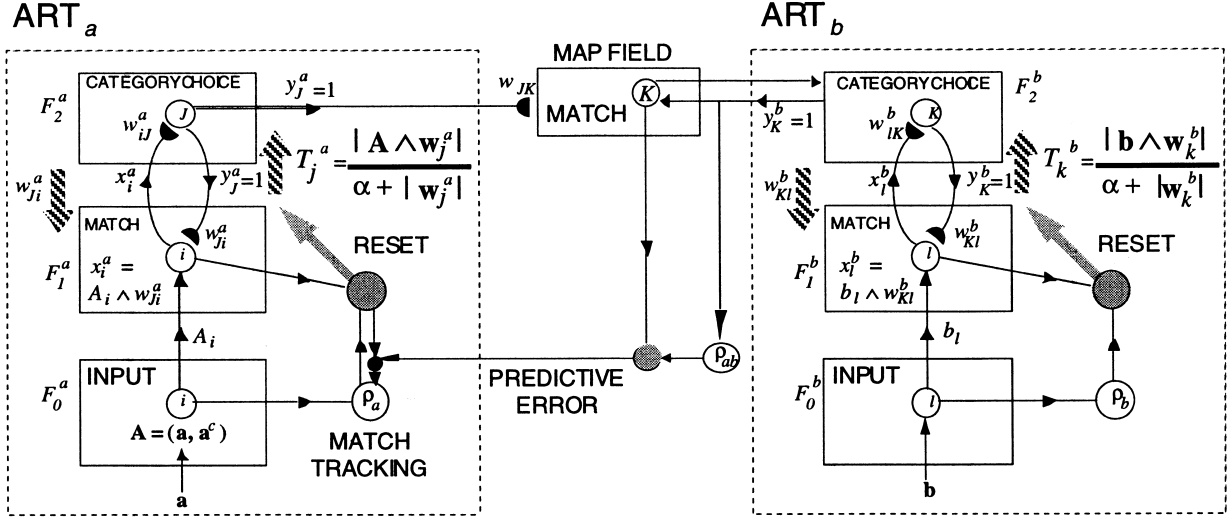


Figure 8. ARTMAP neural network architecture.

nodes $k=1\dots C_b$, let $K=C_b+1$. Node

K is then newly committed: increase C_b by 1.

Go to **Step 4**.

Step 4—Compute the $F_1^a \rightarrow F_2^a$ signal. For $j=1\dots C_a$:

$$T_j^a = \frac{\sum_{i=1}^{2M_a} A_i \wedge w_{ij}^a}{\alpha + \sum_{i=1}^{2M_a} w_{ij}^a}$$

Step 5—Choose an ART_a category J [(i) or (ii)]:

(i) *Committed node:* If $T_j^a \geq T^{a,u}$ for some F_2^a node $j=1\dots C_a$, let J be the lowest

index such that $T_j^a = \max\{T_1^a \dots T_{C_a}^a\}$.

F_1^a activation: $x_i^a \wedge w_{ij}^a$ ($i=1\dots 2M_a$)

If $\sum_{i=1}^{2M_a} x_i^a < \rho_a M_a$, set $T_j^a = 0$

and go to **Step 5**. Else go to **Step 6**.

(ii) *Uncommitted node:* If $T_j^a < T^{a,u}$ for all F_2^a

nodes $j=1\dots C_a$, let $J=C_a+1$. Node

J is then newly committed: increase C_a by 1 and let $\kappa(J)=K$.

Step 6—Match tracking at ART_a in response to a predictive error:

If $\kappa(J)=K$, go to **Step 7**.

If $\kappa(J) \neq K$:

(i) set $\rho_a = \frac{1}{M_a} \left[\sum_{i=1}^{2M_a} x_i^a \right] - \varepsilon$

(raise ART_a vigilance);

(ii) set $T_j^a = 0$ (reset the J th F_2^a node); and

(iii) go to **Step 5**.

Step 7—Resonance: For $i=1\dots 2M_a$ and $l=1\dots M_b$:

Save old weight values: $w_{ij}^{a(old)} = w_{ij}^a$ and $w_{lK}^{b(old)} = w_{lK}^b$

Decrease $F_1^a \leftrightarrow F_2^a$ weights: $w_{ij}^a = A_i \wedge w_{ij}^{a(old)}$

Decrease $F_1^b \leftrightarrow F_2^b$ weights: $w_{lK}^b = b_l \wedge w_{lK}^{b(old)}$

ART_a vigilance recovery: $\rho_a = \bar{\rho}_a$

Step 8—Next input/output pair: Increase n by 1.

$$\text{New input } -A_i = \begin{cases} a_i^{(n)} & \text{if } 1 \leq i \leq M_a \\ 1 - a_i^{(n)} & \text{if } M_a + 1 \leq i \leq 2M_a \end{cases}$$

New output $-b_l = b_l^{(n)}$ ($l=1 \dots M_b$)

Go to **Step 2**.

ARTMAP Testing

During ARTMAP testing, ART_a inputs $\mathbf{a}^{(1)}, \mathbf{a}^{(2)}, \dots$ are presented to the trained system. The goal is to produce site-level mixture output predictions that estimate the *conifer/hardwood/other* fractions for each stand. Initially, $n=0$.

Table 4. ARTMAP Variables

	ART _a		ART _b	
	$i=1 \dots 2M_a$	$j=1 \dots C_a$	$l=1 \dots M_b$	$k=1 \dots C_b$
STM: matching	x_i^a	F_1^a	x_l^b	F_1^b
STM: coding	y_j^a	F_2^a	y_k^b	F_2^b
LTM weights	w_{ij}^a	$F_1^a \leftrightarrow F_2^a$	w_{lK}^b	$F_1^b \leftrightarrow F_2^b$
Bottom-up signal	T_j^a	$F_1^a \rightarrow F_2^a$	T_k^b	$F_1^b \rightarrow F_2^b$

Table 5. ARTMAP Parameters

	Parameter	Domain	Simulation Value
Input components			
Number of ART _a input components	M_a		$M_a=6$
Number of ART _b input components	M_b		$M_b=3$
User-defined constants			
Choice parameter	a	$(0, \infty)$	$a=10^{-6}$
ART _a baseline vigilance	$\bar{\rho}_a$	$[0, 1]$	$\bar{\rho}_a=0$
ART _b vigilance	ρ_b	$[0, 1]$	$\rho_b=0.8$
Match tracking	ε	$ \varepsilon \text{small}$	$\varepsilon=0.01$
System descriptors			
Number of ART _a committed nodes	C_a		Incremental
Number of ART _b committed nodes	C_b		Incremental
$F_1^a \rightarrow F_2^a$ signal to an uncommitted node	$T^{a,u}$	$T_j^a _{w_{ij}=1}$	$\frac{M_a}{a+2M_a} \cong 0.5$
$F_1^b \rightarrow F_2^b$ signal to an uncommitted node	$T^{b,u}$	$T_k^b _{w_{jk}=1}$	$\frac{1}{a+M_b} \cong 0.33$
Index of the active F_2^a node	J	$j=1 \dots C_a$	Maximum T_j^a
Index of the active F_2^b node	K	$k=1 \dots C_b$	Maximum T_k^b
ART _a vigilance	ρ_a	$[\bar{\rho}_a, 1]$	Match tracking
Association between the coding node j and the output class k	$\kappa(j)=k$	$k=1 \dots C_b$	Learning

Test Step 1—New test set input: Increase n by 1.

$$\text{New input } -A_i = \begin{cases} a_i^{(n)} & \text{if } 1 \leq i \leq M_a \\ 1 - a_i^{(n)} & \text{if } M_a + 1 \leq i \leq 2M_a \end{cases}$$

Test Step 2—Compute the $F_1^a \rightarrow F_2^a$ signal: For $j=1 \dots C_a$:

$$T_j^a = \frac{\sum_{i=1}^{2M_a} A_i \wedge w_{ij}^a}{a + \sum_{i=1}^{2M_a} w_{ij}^a}$$

Test Step 3—Choose an ART_a category J :

Let J be smallest F_2^a index such that $T_J^a = \max\{T_1^a \dots T_{C_a}^a\}$.

If $T_J^a < T^{a,u}$, go to **Test Step 1** (no prediction).

Test Step 4—Predict an ART_b category K :

Let $K = \kappa(J)$

Test Step 5—Flow activation top-down through ART_b, producing a normalized system output \mathbf{x}^b : For $l=1 \dots M_b$:

$$x_l^b = \frac{w_{lK}^b}{\sum_{i=1}^{M_b} w_{iK}^b}$$

Test Step 6—Pixel-level output prediction [(i) or (ii)]:

(i) *ARTMAP classification testing:* The output vector \mathbf{x}^b is binary. For example, if

$\mathbf{x}^b = (1, 0, 0) = (\text{con}, \text{hwd}, \text{other})$, then in the final site-level mixture estimate, the pixel casts one *conifer* vote.

(ii) *ARTMAP mixture testing:* The analog output vector \mathbf{x}^b represents the pixel's predicted mixed contribution to the overall composition of the site. For example, if $\mathbf{x}^b = (0.5, 0.3, 0.2) = (\text{con}, \text{hwd}, \text{other})$ is the F_1^b output vector, then, in the site-level mixture prediction, the pixel casts 50% of its vote for *conifer*, 30% for *hardwood*, and 20% for *other*. Recall that *other* = *barren* in the small data set and *other* = *barren* + *brush* in the large data set.

Go to **Test Step 1**, until all test-set pixel-level predictions are recorded.

Test Step 7—Site-level output prediction:

A site-level mixture prediction equals the average prediction of all pixels in the site. That is, the vector that represents the estimated vegetation composition of a site equals the sum of all the output vectors \mathbf{x}^b for that site divided by the number of pixels that are making a prediction for that site.

Varying Mixture Granularity

Table 6 illustrates the effect of varying the ARTMAP parameter ρ_b . This parameter controls the degree of coarse-

Table 6. ARTMAP Mixture RMS Errors as the Vigilance Matching Threshold ρ_b Increases from 0.0 to 0.9, for the Small (No Brush) Data Set without Topographic Correction^a

ρ_b	ARTMAP mixture RMS Error			No. of F_2^a Nodes	No. of F_2^b Nodes
	C	H	Barren		
0.0	0.24	0.12	0.21	48	3
0.4	0.15	0.10	0.13	143	5
0.7	0.15	0.10	0.13	356	11
0.8	0.15	0.10	0.12	508	18
0.9	0.14	0.09	0.12	769	36

^a Also listed are the numbers of internal category nodes used in ART_a and ART_b during training.

ness, or granularity, of the predicted vegetation fractions. When ρ_b is small, the system learns rough estimated fractions, corresponding, approximately, to “low/medium/high” mixture proportions. Larger values of ρ_b create finer output classes and thus more precise predictions, as indicated by the boldface table entries. However, there is a cost in terms of system complexity and memory storage, as indicated by the larger numbers of nodes shown in the right-hand columns of Table 6. A good compromise between accuracy and efficiency sets $\rho_b=0.8$ for the present application. This parameter value was used in all system tests. Thus the RMS error values for that row in Table 6 are the same as the ARTMAP mixture values in Table 2a. For applications in which the field measurements themselves are at a coarser or less accurate level, a smaller value of ρ_b may be more appropriate.

CONCLUSIONS

The newly developed ARTMAP mixture estimation methods provide the best estimates of the fractions of vegetation types within stands, as compared with maximum likelihood classification, ARTMAP classification, and linear mixture models. The tests presented here involve estimation of hardwood and conifer fractions within forest stands in the Plumas National Forest in California. The presence of brush in the understory undermines the estimation of the fraction of overstory components. Topographic correction of the Landsat imagery prior to analysis did not improve results.

This research was supported in part by the National Science Foundation (NSF IRI 94-0165 and NSF SBR 95-13889), by the Office of Naval Research (ONR N00014-95-10409 and ONR N00014-95-10657), and by the Region 5 Remote Sensing Laboratory of the U.S. Forest Service.

REFERENCES

Adams, J. B., Sabol, D. E., Kapos, V., et al. (1995), Classification of multispectral images based on fractions of endmembers: application of land-cover change in the Brazilian Amazon. *Remote Sens. Environ.* 52:137–154.

- Adams, J. B., Smith, M. O., and Gillespie, A. H. (1993), Imaging spectroscopy: interpretation based on spectral mixture analysis. In *Remote Geochemical Analysis: Elemental and Mineralogical Composition 7* (C. M. Pieters and P. Englert, Eds.), Cambridge University Press, New York, pp. 145–166.
- Adams, J. B., Smith, M. O., and Johnson, P. E. (1986), Spectral mixture modeling: a new analysis of rock and soil types at the Viking Lander I site. *J. Geophys. Res.* 91(B8): 8098–8112.
- Carpenter, G. A. (1997), Distributed learning, recognition, and prediction by ART and ARTMAP neural networks. *Neural Networks* 10:1473–1494.
- Carpenter, G. A., Gjaja, M. N., Gopal, S., and Woodcock, C. E. (1997), ART neural networks for remote sensing: vegetation classification from Landsat TM and terrain data. *IEEE Trans. Geosci. Remote Sens.* 35:308–325.
- Carpenter, G. A., Grossberg, S., Markuzon, N., Reynolds, J. H., and Rosen, D. B. (1992), Fuzzy ARTMAP: a neural network architecture for incremental supervised learning of analog multidimensional maps. *IEEE Trans. Neural Networks* 3:698–713.
- Carpenter, G. A., Grossberg, S., and Reynolds, J. H. (1991), ARTMAP: supervised real-time learning and classification of nonstationary data by a self-organizing neural network. *Neural Networks* 4:565–588.
- Civco, D. L. (1989), Topographic normalization of Landsat Thematic Mapper digital imagery. *Photogramm. Eng. Remote Sens.* 55:1303–1309.
- Fisher, P., and Pathirana, S. (1990), An evaluation of fuzzy membership of landcover classes in the suburban zone. *Remote Sens. Environ.* 34:121–132.
- Foody, G. M. (1996), Relating the land-cover composition of mixed pixels to artificial neural network classification output. *Photogramm. Eng. Remote. Sens.* 62:491–499.
- Foody, G. M., Campbell, N. A., Trodd, N. M., and Wood, T. F. (1992), Derivation and applications of probabilistic measures of class membership from maximum likelihood classification. *Photogramm. Eng. Remote. Sens.* 58(9):1335–1341.
- Foody, G. M., Lucas, R. M., Curran, P. J., and Honzak, M. (1997), Non-linear mixture modeling without end-members using an artificial neural network. *Int. J. Remote Sens.* 18:937–954.
- Frew, J. E. (1990), The image processing workbench, Ph.D. dissertation, University of California, Santa Barbara, 303 pp.
- Gu, D., and Gillespie, A. (1998), Topographic normalization of Landsat TM images of forest based on subpixel Sun–canopy–sensor geometry. *Remote Sens. Environ.* 64:166–175.
- Holben, B. N., and Justice, C. O. (1980), The topographic effect on spectral response from nadir-pointing sensors. *Photogramm. Eng. Remote Sens.* 46:1191–1200.
- Justice, C. O., Wharton, S. W., and Holben, B. N. (1981), Application of digital terrain data to quantify and reduce the topographic effect on Landsat data. *Int. J. Remote Sens.* 2:213–230.
- Lee, T. Y., and Kaufman, Y. J. (1986), Non-lambertian effects on remote sensing of surface reflectance and vegetation index. *IEEE Trans. Geosci. Remote Sens.* 24:699–708.
- Li, X., and Strahler A. H. (1992), Geometric–optical bidirectional reflectance modeling of discrete crown vegetation canopy: effect of crown shape and mutual shadowing. *IEEE Trans. Geosci. Remote Sens.* GE-30:276–292.

- Marsh, S. E., Switzer, P., Kowalik, W. S., and Lyon, R. J. P. (1980), Resolving the percentage of component terrains within single resolution elements. *Photogramm. Eng. Remote Sens.* 46:1079–1086.
- Moody, A., Gopal, S., and Strahler, A. H. (1996), Sensitivity of neural networks to subpixel land-cover mixtures in coarse-resolution satellite data. *Remote Sens. Environ.* 58: 329–343.
- Mosier, C. I. (1951), Symposium: the need and the means for cross-validation. 1. Problem and designs of cross-validation. *Ed. Psychol. Measure.* 11:5–11.
- Nalepka, R. F., and Hyde, P. D. (1972), Classifying unresolved objects from simulated space data. In *Proc. of the 8th Int. Symp. on Remote Sens. Environ.*, Environmental Research Institute of Michigan, Ann Arbor, pp. 935–949.
- Naugle, B. I., and Lashlee, J. D. (1992), Alleviating topographic influences on land-cover classifications for mobility and combat modeling. *Photogramm. Eng. Remote Sens.* 58:1217–1221.
- Proy, C., Tanré, D., and Deschamps, P. Y. (1989), Evaluation of topographic effects in remotely sensed data. *Remote Sens. Environ.* 30:21–32.
- Ray, T. W., and Murray, B. C. (1996), Nonlinear spectral mixing in desert vegetation. *Remote Sens. Environ.* 55:59–64.
- Richards, J. A. (1993), *Remote Sensing Digital Image Analysis: An Introduction*, 2nd ed., Springer-Verlag, Berlin, 340 pp.
- Roberts, D. A., Smith, M. O., and Adams, J. B. (1993), Green vegetation, nonphotosynthetic vegetation, and soils in AVIRIS data. *Remote Sens. Environ.* 44:255–269.
- Robinson, V. B. (1988), Some implications of fuzzy set theory applied to geographic databases. *Comput. Environ. Urban Syst.* 12:89–98.
- Smith, J. A., Lin, T. L., and Ranson, K. J. (1980), The Lambertian assumption and Landsat data. *Photogramm. Eng. Remote Sens.* 46:1183–1189.
- Smith, M. O., Ustin, S. L., Adams, J. R., and Gillespie, A. R. (1990), Vegetation in deserts: I. A regional measure of abundance from multispectral images. *Remote Sens. Environ.* 31:1–26.
- Stenback, J. M., and Congalton, R. G. (1990), Using thematic mapper imagery to examine forest understory. *Photogramm. Eng. Remote Sens.* 56:1285–1290.
- Strahler, A. H. (1981), Stratification of natural vegetation for forest and rangeland inventory using Landsat digital imagery and collateral data. *Int. J. Remote Sens.* 2:15–41.
- Strahler, A. N. (1997), Vegetation canopy reflectance modeling—recent developments and remote sensing perspectives. *Remote Sens. Rev.* 15:179–194.
- Strahler, A. H., Woodcock, C. E., and Smith, J. A. (1986), On the nature of models in remote sensing. *Remote Sens. Environ.* 20:121–139.
- Verstraete, M. M., Pinty, B., and Dickinson, R. E. (1990), A physical model of the bidirectional reflectance of vegetation canopies: 1. Theory. *J. Geophys. Res.* 95:11,755–11,765.
- Woodcock, C. E., Collins, J., Gopal, S., et al. (1994), Mapping forest vegetation using Landsat TM imagery and a canopy reflectance model. *Remote Sens. Environ.* 50:240–254.
- Woodcock, C. E., Gopal, S., and Albert, W. (1996), Evaluation of the potential for providing secondary labels in vegetation maps. *Photogramm. Eng. Remote Sens.* 62:393–399.